

The angular sizes of dwarf stars and subgiants

Surface brightness relations calibrated by interferometry

P. Kervella^{1,2}, F. Thévenin³, E. Di Folco⁴ and D. Ségransan⁵

¹ LESIA, UMR 8109, Observatoire de Paris-Meudon, 5, place Jules Janssen, F-92195 Meudon Cedex, France

² European Southern Observatory, Alonso de Cordova 3107, Casilla 19001, Vitacura, Santiago 19, Chile

³ Observatoire de la Côte d'Azur, BP 4229, F-06304 Nice Cedex 4, France

⁴ European Southern Observatory, Karl-Schwarzschild-str. 2, D-85748 Garching, Germany

⁵ Observatoire de Genève, CH-1290 Sauverny, Switzerland

Received date / Accepted date

Abstract. The availability of a number of new interferometric measurements of Main Sequence and subgiant stars makes it possible to calibrate the surface brightness relations of these stars using exclusively direct angular diameter measurements. These empirical laws make it possible to predict the limb darkened angular diameters θ_{LD} of dwarfs and subgiants using their dereddened Johnson magnitudes, or their effective temperature. The smallest intrinsic dispersions of $\sigma \leq 1\%$ in θ_{LD} are obtained for the relations based on the K and L magnitudes, for instance $\log \theta_{LD} = 0.0502(B - L) + 0.5133 - 0.2L$ or $\log \theta_{LD} = 0.0755(V - K) + 0.5170 - 0.2K$. Our calibrations are valid between the spectral types A0 and M2 for dwarf stars (with a possible extension to later types when using the effective temperature), and between A0 and K0 for subgiants. Such relations are particularly useful for estimating the angular sizes of calibrators for long-baseline interferometry from readily available broadband photometry.

Key words. Stars: fundamental parameters, Techniques: interferometric

1. Introduction

The surface brightness (hereafter SB) relations link the emerging flux per solid angle unit of a light-emitting body to its color, or effective temperature. These relations are of considerable astrophysical interest, as a well-defined relation between a particular color index and the surface brightness can provide accurate predictions of the stellar angular diameters. Such predictions are essential for the calibration of long-baseline interferometric observations. We propose in the present paper new and accurate calibrations of the SB-color relations of dwarfs and subgiants based on direct interferometric measurements of nearby members of these two luminosity classes. Our primary purpose is to establish reliable relations that can be used to predict the angular sizes of calibrator stars for long-baseline interferometry.

After defining the surface brightness relations (Sect. 2), we discuss in Sect. 3 the sample of measurements that we selected for our calibrations (interferometric and photometric data). Sect. 4 is dedicated to the calibration of the empirical SB relations, relative to the color indices and to

the effective temperature, for stars of spectral types A0 to M2. We also derive inverse relations to estimate the effective temperature from broadband photometry and angular diameter measurements. As the established relations are intended to be used primarily to predict angular diameters, we discuss in Sect. 5 their associated errors in this context. In Sect. 6, we search for a possible instrumental bias linked to one of the five interferometric instruments represented in our sample. Numerous versions of the SB relations have been established in the literature, mostly for giants and supergiants, and we discuss them in Sect. 7. Main Sequence stars are potentially very good calibrators for long-baseline interferometry, and we discuss this particular application of our SB relations in Sect. 8.

2. Direct and inverse surface brightness relations

By definition, the bolometric surface flux $f \sim L/D^2$ is linearly proportional to T_{eff}^4 , where L is the bolometric flux of the star, D its bolometric diameter and T_{eff} its effective temperature. In consequence, $F = \log f$ is a linear function of the stellar color indices expressed in magnitudes

Send offprint requests to: P. Kervella

Correspondence to: Pierre.Kervella@obspm.fr

(logarithmic scale), and SB relations can be fitted using (for example) the following expressions:

$$F_B = a_0 (B - V)_0 + b_0 \quad (1)$$

$$F_V = a_1 (V - K)_0 + b_1 \quad (2)$$

$$F_H = a_2 (B - H)_0 + b_2 \quad (3)$$

where F_λ is the surface brightness. When considering a perfect blackbody curve, any color can in principle be used to obtain the SB. The index 0 designates the dereddened magnitudes, and the a_i and b_i coefficients represent respectively the slopes and zero points of the different versions of the SB relation. The particular expression of the SB relation $F_V(V - R)$ is also known as the Barnes-Evans (B-E) relation, and is historically the first version to have been calibrated empirically (Barnes, Evans & Pearson 1976). However, the relatively large intrinsic dispersion of the visible B-E relation has led many authors to prefer its infrared counterparts, in particular those based on the K band magnitudes ($\lambda = 2.0 - 2.4 \mu\text{m}$), as infrared wavelengths are less affected by interstellar extinction. The surface brightness F_λ is given by the following expression (Fouqué & Gieren 1997) :

$$F_\lambda = 4.2207 - 0.1 m_{\lambda_0} - 0.5 \log \theta_{\text{LD}} \quad (4)$$

where θ_{LD} is the limb darkened angular diameter, i.e. the angular size of the stellar photosphere.

The linear expressions of the SB can be inverted easily to predict angular diameters, and give linear relations such as:

$$\log \theta_{\text{LD}} = c_1 (V - K) + d_1 - 0.2 V \quad (5)$$

for the $F_V(V - K)$ inversion. We have in this example:

$$c_1 = -2 a_1 \quad (6)$$

$$d_1 = 2 (4.2207 - b_1) \quad (7)$$

In the present paper, we will refer to both the direct and inverse relations as “SB relations”.

3. Selected measurement sample

3.1. Angular diameters

Over the past two years, sixteen new angular diameter measurements of nearby Main Sequence and subgiant stars were obtained with the VLT Interferometer (Glindemann et al. 2000; 2003a; 2003b) equipped with the fiber-based beam combiner VINCI (Kervella et al. 2000; 2003a). To complement this sample, we have searched the literature, and added to our list the measurements related to the stars of luminosity classes IV and V. Most of the visible and infrared interferometers are represented in our sample, with measurements from the NII (*Narrabri Intensity Interferometer*; Hanbury Brown, Davis & Allen 1967), the Mk III (Shao et al. 1988), the PTI

(*Palomar Testbed Interferometer*; Colavita et al. 1999) and the NPOI (*Navy Prototype Optical Interferometer*; Armstrong et al. 1998). Our findings originally included a few lunar occultation measurements, but they were rejected as they were related to variable or multiple stars, or their precision was not sufficient to give them any weight in the fitting process.

To obtain a consistent sample of limb darkened (LD) angular diameters we have retained solely the uniform disk (UD) values from the literature. The conversion of these model-independent measurements to LD values was achieved using the linear LD coefficients u from Claret (2000), and the conversion formula from Hanbury Brown et al. (1974a). These coefficients are broadband, single-parameter approximations of the Kurucz (1992) model atmospheres. They are tabulated for a grid of temperatures, metallicities and surface gravities and we have chosen the closest models to the physical properties of the stars. We have considered a uniform microturbulent velocity of 2 km.s^{-1} for all stars. This single source for limb darkening corrections ensures the self-consistency of our final sample.

3.2. Photometry

All the apparent magnitudes that we have retained from the literature are expressed in the Johnson system. When available, we have preferentially kept the uncertainties given by the original authors, otherwise we adopted arbitrarily a conservative error bar. The U band magnitudes were obtained from Morel et al. (1978) and Mermilliod (1986), and we adopted a ± 0.02 error. The B , V , R and I bands were obtained from several online catalogues available through VIZIER (Ochsenbein, Bauer & Marcout 2000), and we also adopted a ± 0.02 uncertainty. For the J to L infrared bands, references are not so easy to find, as many bright stars are unfortunately absent from the recent infrared surveys, like 2MASS (Cutri et al. 2003) or DENIS (Fouqué et al. 2000). We have relied on the VIZIER database to obtain the infrared magnitudes of our sample of stars. In some cases, the references we used are 30 years old, but many of them have small and reliable uncertainties. The original references of the measurements are given in the footnotes of Table 3.

3.3. Data selection

The SB relations rely on the assumption that stars behave like black bodies, i.e. that their colors are mainly governed by their effective temperature. A severe deviation from this assumption will cause a discrepancy between the actual flux per surface unit and the temperature of the star.

For instance, if there is a second, unresolved star near the main object, its additional flux will bias the spectral energy distribution. For this reason, we have rejected the binary and multiple objects for which separate photometry of the components is not available.

The presence of warm material in the circumstellar environment can also create an excess at infrared wavelengths. While this signature is most useful for identifying the stars surrounded by protoplanetary disks, it creates a bias in the measured color of the star. Some of the stars we selected are surrounded by debris disks (ϵ Eri, α PsA, τ Cet, β Leo), but the contribution of the circumstellar material is negligible, even in the infrared J to L bands. The material surrounding these stars is very cold and radiates mostly in the far infrared domain. We have rejected the measurement of β Pic from Di Folco et al. (in prep.), due to its large uncertainty ($\simeq 10\%$) and to the relatively high density of its edge-on circumstellar disk that could cause significant extinction.

The fast rotating stars can deviate significantly from the black body assumption. As demonstrated by the VINCI observations of the nearby Be star α Eri (Domiciano de Souza et al. 2003), the photosphere of these objects can be deformed by their fast rotation. This creates differential limb darkening between the pole and the equator which appear to have different effective temperatures. This makes it particularly difficult to define the true photometric solid angle subtended by these objects. In addition, many fast rotating stars go through episodes of mass loss, that are likely to create a warm circumstellar environment. The presence of such hot material around the star will create a bias in the flux and color of the star. For these reasons, we have chosen to reject the known fast rotators ($v \sin i \geq 100 \text{ km.s}^{-1}$) and the Be stars from our list.

The very low mass stars *Proxima* (GJ 551, M5.5V) and *Barnard's star* (GJ 699, M4V) have been excluded from our fitting procedures for three reasons. The first is that because of their very low effective temperatures the molecular absorption bands dominate their spectra and lead to a significant discrepancy with the hotter stars. Second, these stars are variable, presenting occasional flares that make it difficult to estimate their magnitudes. Third, they present chromospheric activity that could bias their magnitudes in the U to V colors. However, we have kept these two stars on the SB relation figures for comparison.

The spectroscopic and eclipsing binaries are less useful for the estimation of the surface brightness relation, as it is in general impossible to measure separately the magnitudes of these stars with the required precision. For this reason, we have not included in our sample the angular diameter measurements obtained by spectroscopic or photometric methods. For the interested reader, a rather complete compilation of the measurements using these techniques can be found in the CADARS catalogue by Pasinetti-Fracassini et al. (2001).

3.4. Final sample

We report in Tables 1 and 2 the complete set of measurements that we have considered for our fit. In this table, the angular diameters θ_{UD} (uniform disk) and

θ_{LD} (limb-darkened disk) are expressed in milliarcseconds (mas). The limb darkening conversion coefficient $k = \theta_{\text{LD}}/\theta_{\text{UD}}$ was computed for each star based on the tables of Claret (2000). When a physical parameter was not available in the literature, it has been estimated approximately, and appears in *italic* characters. The observation wavelength λ is given as either the name of the photometric band (V , H , K) or the actual wavelength in μm . The error bar in the angular diameter of the Sun (G2V) has been set arbitrarily to $\pm 0.1\%$. The parallaxes are from the *Hipparcos* catalogue (Perryman et al. 1997), except the α Cen value that was taken from Söderhjelm (1999), who derived it from reprocessed *Hipparcos* data. The interferometer used for each measurement is indicated in the "Instr." column.

4. Surface brightness relations

4.1. Fitting procedure

For each angular diameter measurement θ_{LD} , and based on the observed apparent magnitudes m_{λ} , we have computed the surface brightness F_{λ} in all bands, using the definition of Eq. (4). The resulting F_{λ} values were then fitted relative to the colors ($C_0 - C_1$), using a linear model. This fit was achieved using a classical χ^2 minimization taking into account the errors in both the colors and F_{λ} . The minimized quantity, using the slope a and zero point b as variables, is the reduced χ^2 expression:

$$\chi_{\text{red}}^2(a, b) = \frac{1}{N-2} \sum_{i=1}^N \frac{[(F_0)_i - a (C_0 - C_1)_i - b]^2}{(\sigma_{F_i})^2 + a^2 (\sigma_{C_i})^2} \quad (8)$$

where we have:

- N the total number of measurements in our sample,
- $(F_0)_i$ the surface brightness of star i in band C_0 ,
- $(C_0 - C_1)_i$ the color of the star of index i computed between bands C_0 and C_1 ,
- σ_{C_i} the 1σ error bar in the chosen color of star i ,
- σ_{F_i} the 1σ error bar in the surface brightness F_0 .

The 1σ errors σ_a and σ_b are subsequently estimated from the best fit values a and b by solving numerically the expression:

$$\chi_{\text{red}}^2(a + \sigma_a, b + \sigma_b) = \chi_{\text{red}}^2(a, b) + 1. \quad (9)$$

The solutions of this equation correspond to an elliptic contour, due to the correlation between the a and b variables. It has to be projected on the a and b axis to give the errors. The residuals $\Delta F_i = F_i - F_{\text{model}}$ are used to estimate the intrinsic dispersion $\sigma_{\text{int}}(F)$ of the surface brightness relation from:

$$\sigma_{\text{int}}^2(F) = \frac{1}{N} \sum_{i=1}^N \left[(\Delta F_i)^2 - (\sigma_{F_i})^2 \right] \quad (10)$$

This process gives a total number of 72 (a, b) best fit pairs, with their associated errors (σ_a, σ_b) , and the intrinsic dispersion σ_{int} of the data around the best fit model.

Table 1. Angular diameters of dwarf stars (luminosity class V) measured by long-baseline interferometry (apart from the Sun). They are expressed in mas, and T_{eff} is in K. "Ref.₁" designates the reference used for T_{eff} , $\log g$ and [Fe/H]. When unavailable, the metallicity has been set arbitrarily to the solar value. "Ref.₂" designates the reference used for each angular diameter measurement (expressed in mas). The errors are given in superscript close to each value.

Star	Spect.	π (mas)	Ref. ₁	T_{eff}	$\log g$	[Fe/H]	Instr.	Ref. ₂	λ	θ_{UD}	k	θ_{LD}
α Lyr	A0V	$128.93^{0.55}$	(a,e)	9522	3.98	-0.33	PTI	(8)	K	$3.24^{0.01}$	1.012	$3.28^{0.01}$
α Lyr	A0V	$128.93^{0.55}$	(a,e)	9522	3.98	-0.33	NII	(1)	V	$3.08^{0.07}$	1.046	$3.22^{0.07}$
α Lyr	A0V	$128.93^{0.55}$	(a,e)	9522	3.98	-0.33	Mk III	(4)	0.8	$3.15^{0.03}$	1.028	$3.24^{0.03}$
α Lyr	A0V	$128.93^{0.55}$	(a,e)	9522	3.98	-0.33	Mk III	(4)	0.55	$3.00^{0.05}$	1.046	$3.13^{0.05}$
α CMa A	A1V	$379.21^{1.58}$	(b)	9800	4.30	0.40	NII	(16)	V	$5.60^{0.07}$	1.045	$5.85^{0.07}$
α CMa A	A1V	$379.21^{1.58}$	(b)	9800	4.30	0.40	VLTI	(9)	K	$5.94^{0.02}$	1.012	$6.01^{0.02}$
α CMa A	A1V	$379.21^{1.58}$	(b)	9800	4.30	0.40	Mk III	(4)	0.8	$5.82^{0.11}$	1.027	$5.98^{0.11}$
β Leo	A3V	$90.16^{0.89}$	(g)	8570	4.26	0.20	VLTI	(10)	K	$1.43^{0.03}$	1.015	$1.45^{0.03}$
β Leo	A3V	$90.16^{0.89}$	(g)	8570	4.26	0.20	NII	(1)	V	$1.25^{0.09}$	1.052	$1.31^{0.09}$
α PsA	A3V	$130.08^{0.92}$	(g)	8760	4.22	0.43	NII	(1)	V	$1.98^{0.13}$	1.050	$2.08^{0.14}$
α PsA	A3V	$130.08^{0.92}$	(g)	8760	4.22	0.43	VLTI	(10)	K	$2.20^{0.02}$	1.014	$2.23^{0.02}$
α Cen A	G2V	$747.10^{1.20}$	(k)	5790	4.32	0.20	VLTI	(13)	K	$8.31^{0.02}$	1.024	$8.51^{0.02}$
<i>Sun</i>	G2V			5770								$1919260^{0.1\%}$
τ Cet	G8V	$274.18^{0.80}$	(i)	5400	4.55	-0.40	VLTI	(10)	K	$2.03^{0.03}$	1.024	$2.08^{0.03}$
GJ 166 A	K1V	$198.25^{0.84}$	(a)	5073	4.19	-0.31	VLTI	(15)	K	$1.60^{0.06}$	1.029	$1.65^{0.06}$
α Cen B	K1V	$747.10^{1.20}$	(k)	5260	4.51	0.23	VLTI	(13)	K	$5.86^{0.03}$	1.026	$6.01^{0.03}$
ϵ Eri	K2V	$310.74^{0.85}$	(a)	5052	4.57	-0.15	VLTI	(10)	K	$2.09^{0.03}$	1.027	$2.15^{0.03}$
GJ 105 A	K3V	$138.72^{1.04}$	(a)	4718	4.50	-0.07	PTI	(12)	H, K	$0.91^{0.07}$	1.032	$0.94^{0.07}$
GJ 570 A	K4V	$169.31^{1.67}$	(a)	4533	4.79	0.02	VLTI	(15)	K	$1.19^{0.03}$	1.030	$1.23^{0.03}$
ϵ Ind A	K4.5V	$275.49^{0.69}$	(b)	4500	4.50	-0.10	VLTI	(15)	K	$1.84^{0.02}$	1.030	$1.89^{0.02}$
GJ 380	K7V	$205.23^{0.81}$	(a)	3861	4.68	-0.93	PTI	(12)	H, K	$1.27^{0.04}$	1.018	$1.29^{0.04}$
GJ 191	M1V	$255.12^{0.86}$	(b)	3524	4.87	-0.50	VLTI	(14)	K	$0.68^{0.06}$	1.016	$0.69^{0.06}$
GJ 887	M0.5V	$303.89^{0.87}$	(f)	3645	4.80	0.00	VLTI	(14)	K	$1.37^{0.04}$	1.018	$1.39^{0.04}$
GJ 205	M1.5V	$175.72^{1.20}$	(b)	3626	4.80	0.60	VLTI	(14)	K	$1.12^{0.11}$	1.020	$1.15^{0.11}$
GJ 15 A	M2V	$280.26^{1.05}$	(a)	3721	5.00	-1.40	PTI	(12)	H, K	$0.98^{0.05}$	1.017	$1.00^{0.05}$
GJ 411	M1.5V	$392.52^{0.91}$	(h)	3620	4.90	-0.20	PTI	(12)	H, K	$1.41^{0.03}$	1.019	$1.44^{0.03}$
GJ 699	M4Ve	$549.30^{1.58}$	(a)	3201	5.00	-0.90	PTI	(12)	H, K	$0.99^{0.04}$	1.018	$1.00^{0.04}$
<i>Proxima</i>	M5.5V	$772.33^{2.42}$	(f)	3006	5.19	0.00	VLTI	(14)	K	$1.02^{0.08}$	1.030	$1.05^{0.08}$

- Ref.₁ for T_{eff} , $\log g$ and [Fe/H]: (a) Cenarro et al. (2001); (b) Cayrel de Strobel et al. (1997); (c) Allende Prieto et al. (2002); (d) Gray et al. (2001); (e) Thévenin & Idiart (1999); (f) Ségransan et al. (2003); (g) Ersphamer & North (2003); (h) Cayrel de Strobel et al. (2001); (i) Di Folco et al. (in prep.); (j) Morel et al. (2001); (k) Morel et al. (2000).
- Ref.₂ for angular diameters: (1) Hanbury Brown, Davis & Allen (1974b); (2) Kervella et al. (2004a); (3) Nordgren et al. (2001); (4) Mozurkewich et al. (2003); (5) Thévenin et al. (in prep.); (6) Boden et al. (1998); (7) Nordgren et al. (1999); (8) Ciardi et al. (2001); (9) Kervella et al. (2003b); (10) Di Folco et al. (in prep.); (11) Nordgren et al. (2001); (12) Lane et al. (2001); (13) Kervella et al. (2003c); (14) Ségransan et al. (2003); (15) Ségransan et al. (in prep.); (16) Davis et al. (1986).

From there, we can invert these relations easily to obtain their angular diameter counterparts:

$$\log \theta_{\text{LD}} = c(C_0 - C_1) + d - 0.2 C_0 \quad (11)$$

The slopes and zero points are computed from the (a, b) pairs through:

$$c = -2a, \quad \sigma_c = 2\sigma_a \quad (12)$$

$$d = 2(4.2207 - b), \quad \sigma_d = 2\sigma_b \quad (13)$$

and the intrinsic dispersions $\sigma_{\text{int}}(\log \theta_{\text{LD}})$ are given by:

$$\sigma_{\text{int}}(\log \theta_{\text{LD}}) = 2\sigma_{\text{int}}(F_{\lambda}) \quad (14)$$

The same method was used for the fits using the effective temperature, except that no error bar was considered on the T_{eff} values from the literature (equal weighting),

and we used a second degree polynomial model instead of a linear one. We minimized numerically the following χ^2_{red} expression using a , b , c as variables:

$$\chi^2_{\text{red}}(a, b, c) = \frac{1}{N-3} \sum_{i=1}^N \frac{[F_i - F_{\text{model}}(T_{\text{eff}})_i]^2}{\sigma_F^2} \quad (15)$$

where

$$F_{\text{model}}(T_{\text{eff}})_i = a(\log T_{\text{eff}})_i^2 + b(\log T_{\text{eff}})_i + c. \quad (16)$$

The errors in each of the a , b and c coefficients were not computed, as the correlations existing between these coefficients make it very difficult to determine them accurately. This is justified by the fact that the astrophysical dispersion of the measurements is largely dominant over the 1σ fitting errors of the model, and the systematic

Table 2. Angular diameters of subgiant stars (luminosity class IV) measured by interferometry. The references and notations are given in Table 1.

Star	Spect.	π (mas)	Ref. ₁	T_{eff}	$\log g$	[Fe/H]	Instr.	Ref. ₂	λ	θ_{UD}	k	θ_{LD}
γ Gem	A0IV	$31.12^{2.33}$	(b)	9260	3.60	-0.12	NII	(1)	V	$1.32^{0.09}$	1.047	$1.38^{0.09}$
α CMi A	F5IV-V	$285.93^{0.88}$	(c)	6530	3.96	-0.05	VLTI	(2)	K	$5.38^{0.05}$	1.019	$5.48^{0.05}$
α CMi A	F5IV-V	$285.93^{0.88}$	(c)	6530	3.96	-0.05	NPOI	(11)	V	$5.19^{0.04}$	1.057	$5.49^{0.04}$
α CMi A	F5IV-V	$285.93^{0.88}$	(c)	6530	3.96	-0.05	Mk III	(4)	0.8	$5.32^{0.08}$	1.039	$5.53^{0.08}$
α CMi A	F5IV-V	$285.93^{0.88}$	(c)	6530	3.96	-0.05	Mk III	(4)	0.55	$5.30^{0.11}$	1.057	$5.60^{0.11}$
η Boo	G0IV	$88.17^{0.75}$	(a)	6003	3.62	0.25	VLTI	(5)	K	$2.15^{0.03}$	1.022	$2.20^{0.03}$
η Boo	G0IV	$88.17^{0.75}$	(a)	6003	3.62	0.25	Mk III	(4)	0.8	$2.18^{0.02}$	1.044	$2.27^{0.03}$
η Boo	G0IV	$88.17^{0.75}$	(a)	6003	3.62	0.25	Mk III	(4)	0.55	$2.13^{0.03}$	1.063	$2.26^{0.03}$
η Boo	G0IV	$88.17^{0.75}$	(a)	6003	3.62	0.25	NPOI	(11)	V	$2.17^{0.06}$	1.064	$2.31^{0.06}$
ζ Her A	G0IV	$92.64^{0.60}$	(j)	5820	3.85	0.04	Mk III	(4)	0.8	$2.26^{0.05}$	1.045	$2.36^{0.05}$
ζ Her A	G0IV	$92.64^{0.60}$	(j)	5820	3.85	0.04	Mk III	(4)	0.55	$2.13^{0.03}$	1.065	$2.27^{0.03}$
ζ Her A	G0IV	$92.64^{0.60}$	(j)	5820	3.85	0.04	NPOI	(11)	V	$2.37^{0.08}$	1.065	$2.52^{0.09}$
μ Her	G5IV	$119.05^{0.62}$	(a)	5411	3.87	0.16	Mk III	(4)	0.8	$1.86^{0.04}$	1.049	$1.95^{0.04}$
μ Her	G5IV	$119.05^{0.62}$	(a)	5411	3.87	0.16	Mk III	(4)	0.55	$1.81^{0.03}$	1.070	$1.93^{0.03}$
β Aql	G8IV	$72.95^{0.83}$	(a)	5041	3.04	-0.04	NPOI	(7)	V	$2.07^{0.09}$	1.075	$2.23^{0.10}$
η Cep	K0IV	$69.73^{0.49}$	(a)	5013	3.19	-0.19	NPOI	(7)	V	$2.51^{0.04}$	1.064	$2.67^{0.04}$
δ Eri	K0IV	$110.58^{0.88}$	(a)	4884	3.40	-0.11	VLTI	(5)	K	$2.33^{0.03}$	1.027	$2.39^{0.03}$

errors in these coefficients can thus be considered negligible. The inversion of the resulting T_{eff} based relations is straightforward. With an expression of the form:

$$\log \theta_{\text{LD}} = d(\log T_{\text{eff}})^2 + e(\log T_{\text{eff}}) + f - 0.2C_{\lambda} \quad (17)$$

we have by definition:

$$d = -2a, \quad e = -2b \quad (18)$$

$$f = 2(4.2207 - c) \quad (19)$$

As in the previous case based on colors, the intrinsic dispersions $\sigma_{\text{int}}(\log \theta_{\text{LD}})$ of the angular diameter relations are given by:

$$\sigma_{\text{int}}(\log \theta_{\text{LD}}) = 2\sigma_{\text{int}}(F) \quad (20)$$

In some cases, we could derive only upper limits of the intrinsic dispersion σ_{int} , as it was found to be smaller than the average error of the measurements (in such cases, Eq. 10 gives a negative value for σ_{int}). For these relations, such as $\log \theta_{\text{LD}}(T_{\text{eff}}, L)$, we conclude that the intrinsic dispersion is undetectable at our level of sensitivity.

4.2. Angular diameter relations based on colors

The SB relations for $UBVRIJHKL$ colors are listed in Table 4. They take the form:

$$\log \theta_{\text{LD}}(C_0, C_1) = c_{\lambda}(C_0 - C_1) + d_{\lambda} - 0.2C_0 \quad (21)$$

where C_0 and C_1 are any two distinct colors of the Johnson system. In many cases, the dependence of the zero magnitude limb darkened angular diameter (ZMLD), defined for $C_0 = 0$, as a function of the color is not linear in reality. Thus, the linear model that we fit does not represent the observations well. In this case, we have added a note "nl"

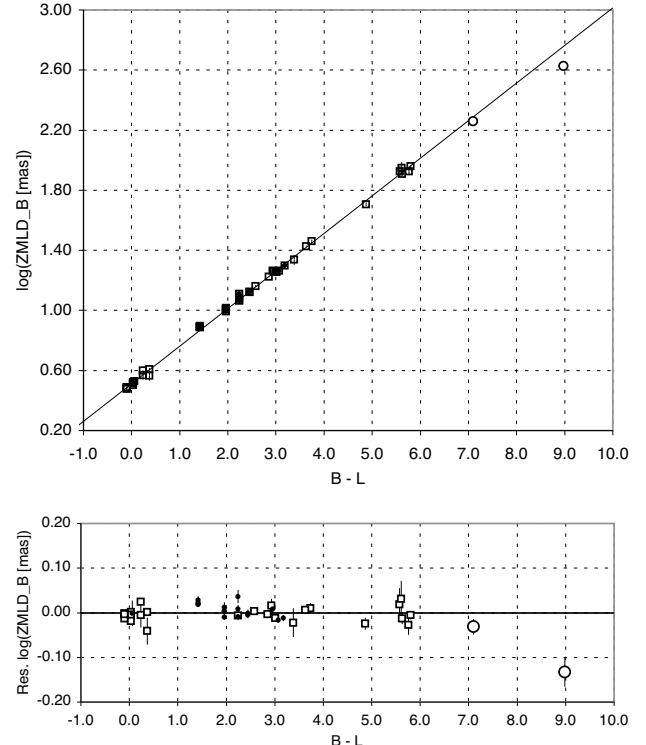


Fig. 1. Linear fit of the surface brightness relation $\log \text{ZMLD}_B(B - L)$ (upper part), and the corresponding residuals (lower part). The intrinsic dispersion in the relation is ± 0.004 on $\log \text{ZMLD}$, equivalent to a systematic error of less than 1% in the predicted angular diameters. The open circles designate GJ 699 and *Proxima*, which were excluded from the fitting procedure.

after the obtained residual dispersion. The non-linear relations should preferably not be used for predictions, though the stated dispersions include the non-linearity.

Table 3. Apparent magnitudes of the dwarf stars (upper part) and subgiants (lower part) of our sample. The uncertainty adopted for each apparent magnitude value is given in superscript.

Star	$m_U^{(a)}$	$m_B^{(b)}$	$m_V^{(b)}$	$m_R^{(c)}$	$m_I^{(c)}$	$m_J^{(d)}$	$m_H^{(d)}$	$m_K^{(d)}$	$m_L^{(d)}$
α Lyr	$0.03^{0.02}$	$0.03^{0.02}$	$0.03^{0.02}$	$0.04^{0.02}$	$0.03^{0.02}$	$0.00^{0.02}$	$0.00^{0.01}$	$0.00^{0.01}$	$0.00^{0.01}$
α CMa A	$-1.51^{0.02}$	$-1.46^{0.02}$	$-1.46^{0.02}$	$-1.46^{0.02}$	$-1.45^{0.02}$	$-1.34^{0.03}$	$-1.32^{0.03}$	$-1.32^{0.02}$	$-1.36^{0.03}$
β Leo	$2.30^{0.02}$	$2.22^{0.02}$	$2.14^{0.02}$	$2.08^{0.02}$	$2.06^{0.02}$	$2.02^{0.01}$	$1.99^{0.09}$	$1.86^{0.09}$	$1.86^{0.09}$
α PsA	$1.31^{0.02}$	$1.25^{0.02}$	$1.16^{0.02}$	$1.10^{0.02}$	$1.08^{0.02}$	$1.06^{0.05}$	$1.05^{0.06}$	$0.99^{0.03}$	$1.01^{0.07}$
α Cen A	$0.92^{0.02}$	$0.70^{0.02}$	$-0.01^{0.02}$			$-1.16^{0.02}$	$-1.39^{0.09}$	$-1.50^{0.02}$	$-1.55^{0.09}$
$Sun^{(e)}$	$-25.98^{0.02}$	$-26.12^{0.02}$	$-26.75^{0.02}$	$-27.12^{0.02}$	$-27.48^{0.02}$	$-27.86^{0.02}$	$-28.20^{0.02}$	$-28.22^{0.02}$	
τ Cet	$4.43^{0.02}$	$4.22^{0.02}$	$3.50^{0.02}$	$2.88^{0.01}$	$2.41^{0.01}$	$2.11^{0.01}$	$1.73^{0.01}$	$1.66^{0.01}$	$1.64^{0.01}$
GJ 166 A	$5.69^{0.02}$	$5.25^{0.02}$	$4.43^{0.02}$	$3.72^{0.01}$	$3.27^{0.01}$	$2.91^{0.03}$	$2.46^{0.01}$	$2.39^{0.02}$	$2.30^{0.02}$
α Cen B	$2.86^{0.02}$	$2.21^{0.02}$	$1.33^{0.02}$			$-0.01^{0.02}$	$-0.49^{0.09}$	$-0.60^{0.02}$	$-0.63^{0.09}$
ϵ Eri	$5.19^{0.02}$	$4.61^{0.02}$	$3.73^{0.02}$	$3.01^{0.02}$	$2.54^{0.02}$	$2.23^{0.03}$	$1.75^{0.03}$	$1.67^{0.01}$	$1.60^{0.05}$
GJ 105 A	$7.58^{0.02}$	$6.81^{0.02}$	$5.83^{0.02}$	$4.99^{0.02}$	$4.46^{0.02}$	$4.07^{0.03}$	$3.52^{0.03}$	$3.45^{0.03}$	$3.43^{0.03}$
GJ 570 A	$7.88^{0.02}$	$6.82^{0.02}$	$5.71^{0.02}$	$4.72^{0.02}$	$4.18^{0.02}$	$3.82^{0.02}$	$3.27^{0.02}$	$3.15^{0.02}$	$3.11^{0.02}$
ϵ Ind A	$6.74^{0.02}$	$5.75^{0.02}$	$4.69^{0.02}$	$3.81^{0.02}$	$3.25^{0.02}$	$2.83^{0.02}$	$2.30^{0.02}$	$2.18^{0.02}$	$2.12^{0.02}$
GJ 380	$9.23^{0.02}$	$7.94^{0.02}$	$6.59^{0.02}$	$5.36^{0.02}$	$4.56^{0.02}$	$3.98^{0.03}$	$3.32^{0.03}$	$3.19^{0.03}$	$3.11^{0.03}$
GJ 191	$11.64^{0.02}$	$10.40^{0.02}$	$8.86^{0.02}$			$5.77^{0.02}$	$5.27^{0.02}$	$5.05^{0.02}$	$4.86^{0.02}$
GJ 887	$9.99^{0.02}$	$8.83^{0.02}$	$7.35^{0.02}$			$4.20^{0.02}$	$3.60^{0.02}$	$3.36^{0.02}$	$3.20^{0.02}$
GJ 205	$10.63^{0.02}$	$9.44^{0.02}$	$7.97^{0.02}$	$6.53^{0.02}$	$5.39^{0.02}$	$4.77^{0.02}$	$4.06^{0.02}$	$3.86^{0.02}$	$3.83^{0.02}$
GJ 15 A	$10.88^{0.02}$	$9.63^{0.02}$	$8.07^{0.02}$	$6.72^{0.02}$	$5.53^{0.02}$	$4.86^{0.03}$	$4.25^{0.03}$	$4.02^{0.02}$	$3.87^{0.03}$
GJ 411	$10.13^{0.02}$	$9.00^{0.02}$	$7.49^{0.02}$	$5.98^{0.02}$	$4.76^{0.02}$	$4.13^{0.03}$	$3.56^{0.03}$	$3.35^{0.03}$	$3.20^{0.03}$
GJ 699	$12.57^{0.02}$	$11.28^{0.02}$	$9.54^{0.02}$	$7.71^{0.02}$	$6.10^{0.02}$	$5.30^{0.02}$	$4.77^{0.02}$	$4.52^{0.02}$	$4.18^{0.02}$
<i>Proxima</i>	$14.56^{0.02}$	$13.02^{0.02}$	$11.05^{0.02}$	$8.68^{0.02}$	$6.42^{0.02}$	$5.33^{0.02}$	$4.73^{0.02}$	$4.36^{0.03}$	$4.04^{0.02}$
γ Gem	$1.97^{0.02}$	$1.92^{0.02}$	$1.92^{0.02}$	$1.86^{0.02}$	$1.87^{0.02}$	$1.87^{0.02}$	$1.83^{0.02}$	$1.85^{0.03}$	$1.87^{0.09}$
α CMi A	$0.82^{0.02}$	$0.79^{0.02}$	$0.37^{0.02}$	$-0.05^{0.02}$	$-0.28^{0.02}$	$-0.40^{0.03}$	$-0.60^{0.03}$	$-0.65^{0.03}$	$-0.68^{0.03}$
η Boo	$3.46^{0.02}$	$3.26^{0.02}$	$2.68^{0.02}$	$2.24^{0.02}$	$1.95^{0.02}$	$1.67^{0.02}$	$1.39^{0.01}$	$1.35^{0.01}$	$1.30^{0.02}$
ζ Her A	$3.67^{0.02}$	$3.46^{0.02}$	$2.81^{0.02}$	$2.30^{0.02}$	$1.98^{0.02}$	$1.77^{0.01}$	$1.42^{0.01}$	$1.38^{0.01}$	$1.30^{0.06}$
μ Her	$4.57^{0.02}$	$4.17^{0.02}$	$3.42^{0.02}$	$2.89^{0.02}$	$2.51^{0.02}$	$2.13^{0.01}$	$1.80^{0.01}$	$1.74^{0.01}$	$1.72^{0.02}$
β Aql	$5.07^{0.02}$	$4.58^{0.02}$	$3.72^{0.02}$	$3.06^{0.02}$	$2.57^{0.02}$	$2.19^{0.02}$	$1.70^{0.01}$	$1.65^{0.02}$	$1.61^{0.02}$
η Cep	$4.96^{0.02}$	$4.35^{0.02}$	$3.43^{0.02}$	$2.76^{0.02}$	$2.27^{0.02}$	$1.80^{0.05}$		$1.22^{0.02}$	$1.17^{0.09}$
δ Eri	$5.13^{0.02}$	$4.46^{0.02}$	$3.54^{0.02}$	$2.82^{0.02}$	$2.32^{0.02}$	$1.95^{0.01}$	$1.49^{0.02}$	$1.40^{0.01}$	$1.36^{0.02}$

– References:

- (a) Morel et al. (1978), Mermilliod (1986).
- (b) Morel et al. (1978), Hoffleit & Warren (1991), Perryman et al. (1997).
- (c) Morel et al. (1978), Bessell et al. (1998), Ducati et al. (2002).
- (d) Glass (1974), Glass (1975), Mould & Hyland (1976), Morel et al. (1978), Leggett (1992), Ducati et al. (2002), Kidger & Martín-Luis (2003), the 2MASS catalogue (Cutri et al. 2003).
- (e) We referred to Colina et al. (1996) for the apparent magnitudes of the Sun.

In theory, there should be a perfect diagonal symmetry between the dispersions listed in Table 4. In reality, the symmetry is only approximate, because C_0 and C_1 are not symmetric in the expression of $\log \theta_{LD}(C_0, C_1)$. Therefore, an increased dispersion of the apparent magnitudes in one band C_1 will be reflected preferentially in the $\theta_{LD}(C_0, C_1)$ dispersion, rather than in $\theta_{LD}(C_1, C_0)$. For this reason, we provide both versions in Table 4, including the quasi-symmetric pairs. The best relations based on the K band (showing residual dispersions below 1% on the angular diameter θ_{LD}) are the following:

$$\log \theta_{LD} = 0.0535(B - K) + 0.5159 - 0.2K \quad (22)$$

$$\log \theta_{LD} = 0.0755(V - K) + 0.5170 - 0.2K. \quad (23)$$

and the best relations for the L band are:

$$\log \theta_{LD} = 0.0412(U - L) + 0.5167 - 0.2L \quad (24)$$

$$\log \theta_{LD} = 0.0502(B - L) + 0.5133 - 0.2L \quad (25)$$

$$\log \theta_{LD} = 0.0701(V - L) + 0.5139 - 0.2L \quad (26)$$

$$\log \theta_{LD} = 0.1075(R - L) + 0.5128 - 0.2L. \quad (27)$$

These expressions are valid at least over the range of colors defined by our sample (Tables 1 and 2). In terms of spectral types, the angular diameter predictions can be considered reliable between A0 and M2 for dwarfs, and between A0 and K0 for subgiants. There are indications (Fig. 1) that the infrared relations are valid down to the spectral type M4V of GJ 699, but show some discrepancy for the M5.5V star *Proxima*. The established relations are likely to be valid also for subgiants of spectral types later than K0IV, but this cannot be verified from our sample. It should be stressed that they are applicable only to single stars, and the presence of a non-resolved stellar companion

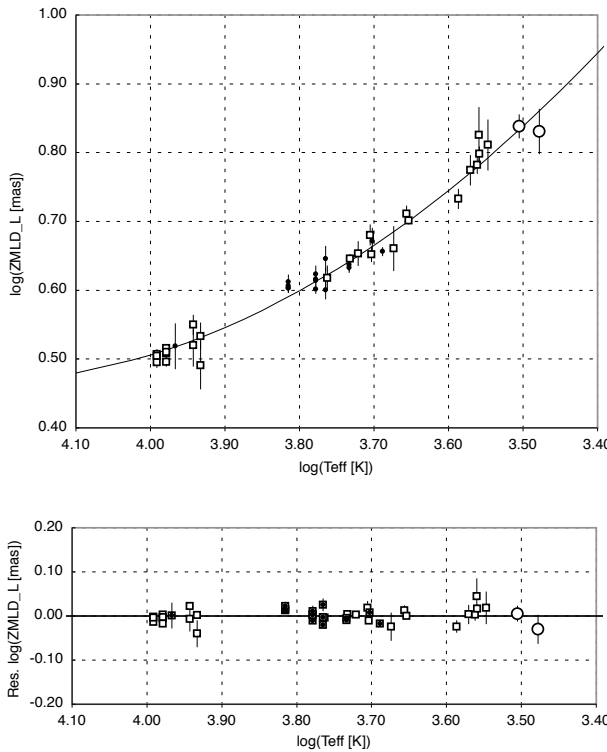


Fig. 3. Second degree polynomial fit of $ZMLD_L(\log T_{\text{eff}})$ (upper part) and the corresponding residuals (lower part). The coefficients are given in Table 5, and correspond to a relation of the form $\log ZMLD_L = d(\log T_{\text{eff}})^2 + e(\log T_{\text{eff}}) + f$. The open circles designate GJ 699 and *Proxima*, which were excluded from the fit (see Sect. 3.3), though they are consistent with the model within their error bars.

contributing a significant fraction of the measured flux will bias the predicted angular diameters. As more than half of the Main Sequence stars are binary or multiple stars, care should be taken in the application of these relations.

4.3. Angular diameter relations based on effective temperatures

Table 5 gives the best fit model coefficients for the relations $\theta_{\text{LD}}(T_{\text{eff}}, C_{\lambda})$, defined as:

$$\log \theta_{\text{LD}} = d(\log T_{\text{eff}})^2 + e(\log T_{\text{eff}}) + f - 0.2 C_{\lambda} \quad (28)$$

The smallest residuals are obtained for the relations based on T_{eff} and the K or L magnitudes, with an upper limit on the 1σ dispersion of 1.0% (the true dispersion is undetectable from our data):

$$\log \theta_{\text{LD}} = 0.8470 x^2 - 7.0790 x + 15.2731 - 0.2 K$$

$$\log \theta_{\text{LD}} = 0.6662 x^2 - 5.6609 x + 12.4902 - 0.2 L$$

where $x = \log T_{\text{eff}}$. The range of validity of the T_{eff} based relations is 3600–10000 K for dwarfs, and 4900–9500 K for subgiants. As shown in Fig. 3, there are indications that

Table 5. SB relations using the magnitude C_{λ} and the effective temperature T_{eff} of the star to obtain the limb darkened angular diameter θ_{LD} (in mas): $\log \theta_{\text{LD}}(T_{\text{eff}}, C_{\lambda}) = d(\log T_{\text{eff}})^2 + e \log T_{\text{eff}} + f - 0.2 C_{\lambda}$. The 1σ residual dispersions are given in percents of the LD angular diameter.

C_{λ}	σ	d	e	f
U	5.93%	5.6391	-46.4505	96.0513
B	6.33%	3.6753	-30.9671	65.5421
V	5.90%	3.0415	-25.4696	53.7010
R	4.76%	2.1394	-18.0221	38.3497
I	2.28%	0.9847	-8.7985	19.9281
J	1.19%	0.9598	-8.3451	18.5204
H	1.38%	1.1684	-9.6156	20.2779
K	$\leq 1.00\%$	0.8470	-7.0790	15.2731
L	$\leq 1.00\%$	0.6662	-5.6609	12.4902

the infrared relations are valid for dwarfs with T_{eff} down to ~ 3000 K.

4.4. $T_{\text{eff}}(\theta_{\text{LD}}, m_{\lambda})$ relations

By inverting the relations established in Sect. 4.3, it is possible to predict the effective temperature of the observed stars based on their angular diameter and broadband magnitude in a single band. As in the previous sections, we assume zero interstellar extinction, and the relations are valid only for dereddened magnitudes. The formulation of the $T_{\text{eff}}(\theta_{\text{LD}}, m_{\lambda})$ laws is easily derived analytically. From Eq. 28, we obtain $\log T_{\text{eff}}$ through the expression:

$$\log T_{\text{eff}} = \frac{-\sqrt{4d \log \theta_{\text{LD}} + 0.8d C_{\lambda} + e^2 - 4df} - e}{2d} \quad (29)$$

that can be rewritten as

$$\log T_{\text{eff}} = -\sqrt{g \log \theta_{\text{LD}} + h C_{\lambda} + i} + j \quad (30)$$

where

$$g = \frac{1}{d}, \quad h = \frac{0.2}{d}, \quad (31)$$

$$i = \frac{e^2}{4d^2} - \frac{f}{d}, \quad j = \frac{-e}{2d}. \quad (32)$$

The intrinsic dispersion of the $\log T_{\text{eff}}$ relations can be approximated from the intrinsic dispersion of the $\log \theta_{\text{LD}}$ relations, as we have $\sigma_{\text{int}}(\log \theta_{\text{LD}}) \ll 1$:

$$\sigma_{\text{int}}(\log T_{\text{eff}}) = 0.5 \sqrt{g} \sigma_{\text{int}}(\log \theta_{\text{LD}}) \quad (33)$$

The corresponding coefficients and dispersions are given in Table 6. The K band relation presents the smallest intrinsic dispersion ($\sigma \leq 0.60\%$), corresponding to a systematic uncertainty of less than 40 K in the predicted temperature of a G2V star:

$$\log T_{\text{eff}} = 4.1788 - \sqrt{1.1806 \log \theta_{\text{LD}} + 0.2361 K - 0.5695}$$

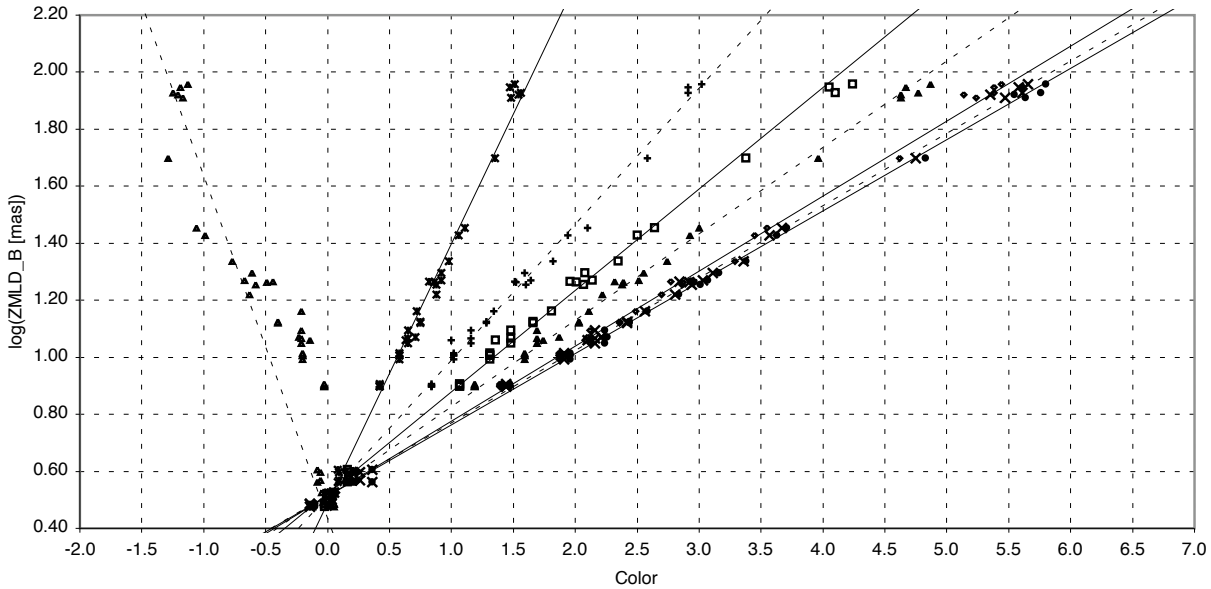


Fig. 2. Johnson B band $ZMLD_B$ relations as a function of color. The errors bars have been omitted for clarity, and the fitted models are represented alternatively as solid and dashed lines. From left to right, using the colors: $(B - U)$, $(B - V)$, $(B - R)$, $(B - I)$, $(B - J)$, $(B - H)$, $(B - K)$, $(B - L)$. A clear non-linearity is visible on the $(B - U)$ based relation.

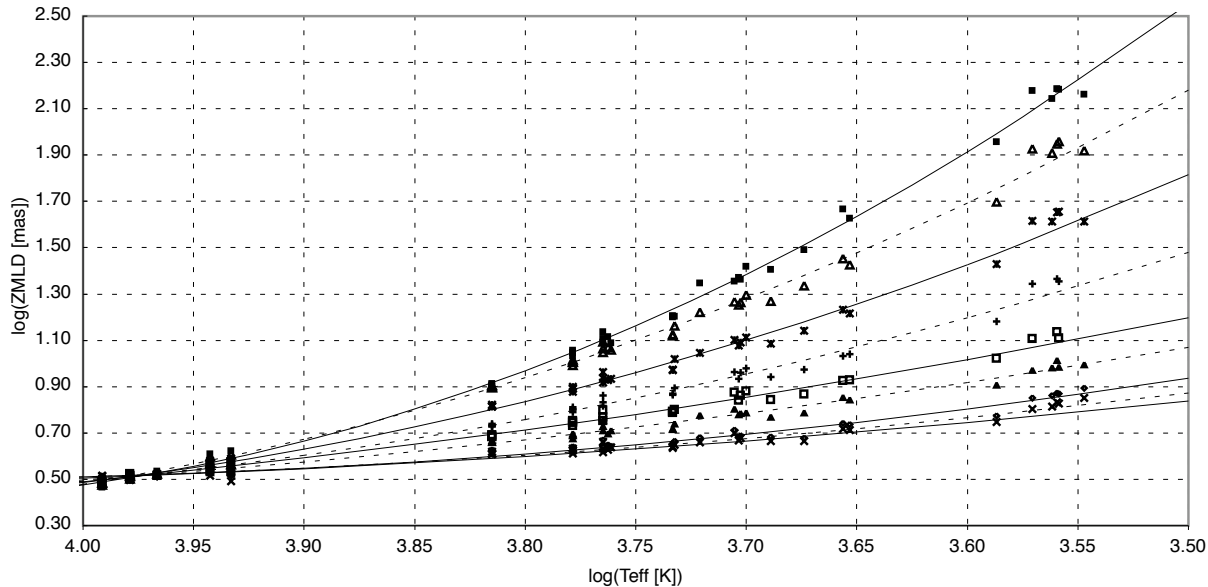


Fig. 4. $ZMLD_\lambda$ relations as a function of the effective temperature. The error bars have been omitted for clarity, and the fitted models are represented alternatively as solid and dashed lines. From top to bottom, using the zero magnitude reference colors U , B , V , R , I , J , H , K and L .

However, we would like to stress that the uncertainty in the measured apparent magnitudes can easily be dominant, as a ± 0.03 error in K will translate into a $\pm 1.7\%$ error in T_{eff} , nearly three times as large as the intrinsic dispersion.

Considering that photometry at an absolute level of ± 0.01 is not available for all stars, the T_{eff} predictions from

different bands can be averaged, taking carefully into account the statistical and systematic errors of each relation used, in order to reach the intrinsic dispersion level. In addition, such an averaging process should not be done for stars affected by interstellar or circumstellar extinction, as it will affect differently each photometric band.

Table 4. Surface brightness relations using $UBVRIJHKL$ based colors to obtain the limb darkened angular diameter θ_{LD} (in mas) as a function of the magnitude and color of the star through: $\log \theta_{\text{LD}}(C_0, C_1) = c_\lambda(C_0 - C_1) + d_\lambda - 0.2 C_0$. The residual dispersions are given in percents of the LD angular diameter. The 1σ errors in each coefficient are given in superscript, multiplied by 1000 to reduce the length of each line, i.e. $0.5822^{3.2}$ stands for 0.5822 ± 0.0032 . When the data depart significantly from our linear fit and present a detectable non-linearity, the dispersion is mentioned in italic characters, and we have added the note "nl". The dispersions smaller than 5% are mentioned in bold characters: they mark the relations that are the most suitable for predicting stellar angular sizes.

$C_0 \downarrow$	$C_1 \rightarrow U$	B	V	R	I	J	H	K	L
c_U		1.2701 ^{11.8}	0.5822 ^{3.2}	0.3925 ^{1.7}	0.3178 ^{1.1}	0.2805 ^{1.0}	0.2509 ^{0.8}	0.2437 ^{0.8}	0.2407 ^{0.8}
d_U		0.6607 ^{7.9}	0.5532 ^{4.5}	0.5393 ^{3.5}	0.5384 ^{3.1}	0.5351 ^{3.0}	0.5206 ^{2.9}	0.5217 ^{2.7}	0.5184 ^{2.9}
σ_U		57.8% nl	17.9% nl	10.6% nl	7.88% nl	5.05% nl	3.06%	2.76%	1.92%
c_B	-1.0923 ^{10.4}		0.9095 ^{6.9}	0.4771 ^{2.2}	0.3557 ^{1.4}	0.3029 ^{1.0}	0.2630 ^{0.8}	0.2538 ^{0.7}	0.2501 ^{0.9}
d_B	0.6542 ^{7.0}		0.4889 ^{1.1}	0.5116 ^{0.1}	0.5235 ^{0.1}	0.5242 ^{0.1}	0.5134 ^{1.0}	0.5158 ^{0.1}	0.5133 ^{0.1}
σ_B	59.2% nl		9.17% nl	4.75% nl	4.98% nl	3.07%	1.89%	$\leq 1.00\%$	$\leq 1.00\%$
c_V	-0.3846 ^{2.3}	-0.7083 ^{7.4}		0.7900 ^{8.4}	0.4550 ^{2.9}	0.3547 ^{2.0}	0.2893 ^{1.6}	0.2753 ^{1.4}	0.2694 ^{1.4}
d_V	0.5513 ^{3.4}	0.4889 ^{5.7}		0.5217 ^{6.4}	0.5332 ^{4.0}	0.5310 ^{3.6}	0.5148 ^{3.2}	0.5175 ^{2.9}	0.5146 ^{3.1}
σ_V	18.0% nl	9.18% nl		8.53% nl	8.30% nl	4.75%	1.85%	1.01%	$\leq 1.00\%$
c_R	-0.1966 ^{1.0}	-0.2792 ^{1.7}	-0.5842 ^{5.1}		0.7404 ^{6.4}	0.4647 ^{3.2}	0.3405 ^{2.5}	0.3158 ^{1.9}	0.3041 ^{1.8}
d_R	0.5351 ^{2.4}	0.5109 ^{3.0}	0.5251 ^{4.7}		0.5570 ^{5.2}	0.5392 ^{4.0}	0.5119 ^{3.8}	0.5158 ^{3.1}	0.5144 ^{3.3}
σ_R	11.1% nl	5.02% nl	8.63% nl		14.5% nl	8.43% nl	2.88%	2.05%	2.52%
c_I	-0.1210 ^{0.7}	-0.1587 ^{1.1}	-0.2609 ^{2.0}	-0.5998 ^{7.6}		0.9079 ^{19.8}	0.4318 ^{6.0}	0.3833 ^{4.5}	0.3707 ^{4.6}
d_I	0.5351 ^{1.9}	0.5207 ^{2.3}	0.5296 ^{2.8}	0.5416 ^{4.7}		0.5233 ^{7.6}	0.5089 ^{4.4}	0.5140 ^{3.7}	0.5097 ^{4.0}
σ_I	8.30% nl	5.34% nl	8.73% nl	12.1% nl		10.8% nl	5.83% nl	3.84%	3.30%
c_J	-0.0818 ^{0.6}	-0.1043 ^{0.9}	-0.1581 ^{1.4}	-0.2842 ^{3.2}	-0.7198 ^{16.9}		0.6280 ^{16.0}	0.5214 ^{10.6}	0.4840 ^{9.4}
d_J	0.5325 ^{1.9}	0.5216 ^{2.2}	0.5276 ^{2.4}	0.5299 ^{3.2}	0.5197 ^{6.5}		0.4990 ^{5.8}	0.5066 ^{4.9}	0.5078 ^{4.8}
σ_J	5.13% nl	3.12%	4.98%	7.26% nl	10.9% nl		10.44% nl	5.86% nl	4.08%
c_H	-0.0513 ^{0.5}	-0.0625 ^{0.6}	-0.0892 ^{0.9}	-0.1376 ^{1.8}	-0.2290 ^{4.0}	-0.4312 ^{12.1}		1.8747 ^{58.8}	1.1714 ^{27.7}
d_H	0.5189 ^{1.6}	0.5138 ^{1.8}	0.5145 ^{1.9}	0.5138 ^{2.3}	0.5093 ^{2.9}	0.5013 ^{4.4}		0.5352 ^{7.5}	0.5271 ^{6.2}
σ_H	2.67%	1.24%	1.12%	2.06%	5.53% nl	10.31% nl		17.2% nl	13.0% nl
c_K	-0.0440 ^{0.4}	-0.0535 ^{0.6}	-0.0755 ^{0.8}	-0.1144 ^{1.4}	-0.1805 ^{2.8}	-0.3192 ^{7.4}	-1.7040 ^{55.1}		3.0857 ^{33.9}
d_K	0.5202 ^{1.6}	0.5159 ^{1.6}	0.5170 ^{1.7}	0.5168 ^{1.9}	0.5149 ^{2.3}	0.5089 ^{3.4}	0.5336 ^{7.0}		0.6258 ^{3.6}
σ_K	2.58%	$\leq 1.00\%$	$\leq 1.00\%$	1.60%	3.67%	5.87% nl	17.6% nl		26.9% nl
c_L	-0.0412 ^{0.5}	-0.0502 ^{0.6}	-0.0701 ^{0.8}	-0.1075 ^{1.4}	-0.1696 ^{2.9}	-0.2826 ^{6.4}	-0.9843 ^{24.1}	-2.8950 ^{115.7}	
d_L	0.5167 ^{1.7}	0.5133 ^{1.8}	0.5139 ^{1.9}	0.5128 ^{2.1}	0.5101 ^{2.5}	0.5081 ^{3.3}	0.5245 ^{5.4}	0.5309 ^{12.4}	
σ_L	$\leq 1.00\%$	$\leq 1.00\%$	$\leq 1.00\%$	$\leq 1.00\%$	2.43%	3.61%	13.1% nl	26.3% nl	

Table 6. $T_{\text{eff}}(\theta_{\text{LD}}, m_\lambda)$ relations to obtain the effective temperature: $\log T_{\text{eff}} = -\sqrt{g \log \theta_{\text{LD}} + h C_\lambda + i + j}$. The 1σ residual dispersions are given in percents of the effective temperature T_{eff} (expressed in K).

C_λ	σ	g	h	i	j
U	1.19%	0.1773	0.0355	-0.0703	4.1186
B	1.57%	0.2721	0.0544	-0.0850	4.2128
V	1.61%	0.3288	0.0658	-0.1249	4.1870
R	1.57%	0.4674	0.0935	-0.1848	4.2120
I	1.13%	1.0155	0.2031	-0.2788	4.4675
J	0.60%	1.0419	0.2084	-0.3975	4.3472
H	0.63%	0.8559	0.1712	-0.4230	4.1149
K	$\leq 0.60\%$	1.1806	0.2361	-0.5695	4.1788
L	$\leq 0.60\%$	1.5010	0.3002	-0.6977	4.2486

4.5. Metallicity

A possible source of natural dispersion of the SB relations is the presence of deep absorption lines in the spectra of the stars. This effect is stronger for stars that have a high metal content. However, as shown in Fig. 5, there is no clear evidence of a correlation between the residuals of the least dispersed relation $\theta_{\text{LD}}(L, B - L)$ and the metallicity [Fe/H]. This is an indication that our SB relations are valid at least for metallicities between -0.5 and +0.5 dex, and probably also for lower values. The two metal-deficient stars of Fig. 5 are GJ 15 A ([Fe/H] = -1.40 dex) and GJ 699 ([Fe/H] = -0.90 dex, not included in our fits). For typical stars of the solar neighborhood our relations are thus always applicable.

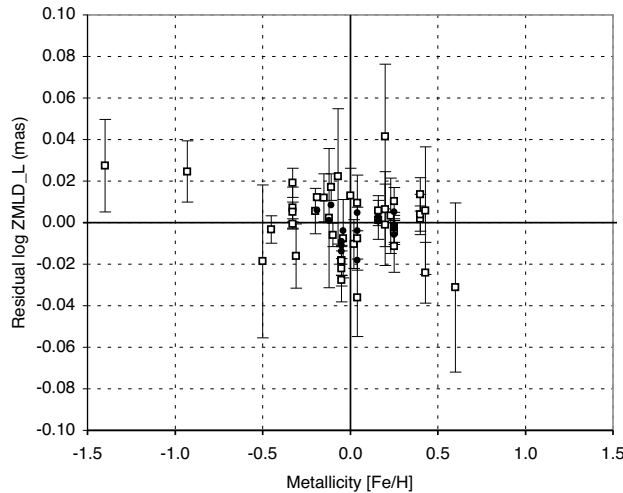


Fig. 5. Residuals of the fit of $ZMLD_L(L, B - L)$ as a function of the metallicity $[\text{Fe}/\text{H}]$ of the star. Dwarfs are represented by open squares, and subgiants by solid dots. No correlation is visible among the stars of our sample.

5. Sources of uncertainty in the predicted diameters

Several observational and astrophysical sources of uncertainty add up to create the total error in the predicted angular diameters:

- *intrinsic dispersion of the empirical relation*: as discussed above, the best relations have intrinsic dispersions below 1%. It should be stressed that their predictions cannot be averaged to reduce this systematic uncertainty. However, the predictions from independent colors (such as $V - K$ and $B - L$) can be averaged to reduce the statistical uncertainty in the predictions due to the errors in the photometric measurements. In this process, the systematic uncertainties of each relation *cannot* be reduced and have to be carefully taken into account. This is essential as the calibrations have been obtained for all colors from the same sample of stars, and the resulting systematic errors are therefore highly correlated.
- *uncertainties in the apparent magnitudes*: combining the high precision magnitudes available in the visible with the infrared magnitudes produced by the 2MASS and DENIS surveys should make it possible to retrieve the visible-infrared color indices with a precision better than ± 0.02 mag. However, we would like to stress that the uncertainty in the apparent magnitude measurements can easily be the largest contributor to the predicted angular diameter errors. The true errors in the photometric measurements have to be estimated accurately in order to obtain reasonable uncertainties in the predicted angular sizes.
- *interstellar extinction and circumstellar matter*: for the sample of nearby stars that was considered for our fits, the interstellar extinction is negligible: apart

from γ Gem at 32 pc, all stars are located closer than 15 pc. However, our SB relations are strictly valid only for extinction-corrected magnitudes. The uncertainty in the assumed color excess $E(B - V)$ (for instance) will translate into an additional uncertainty in the dereddened magnitudes. The presence of a significant amount of circumstellar matter around the star will also affect its spectral properties, and can be difficult to detect.

6. Comparison between interferometers

The residuals of the fits of the least dispersed relations (based on infrared colors) allow us to examine if systematic discrepancies are detectable between the five interferometers represented in our sample. For each instrument we have computed the average residuals of its measurements, and the 1σ error resulting from the averaging of their respective errors. The results are presented in Table 7.

We observe that the average residuals are below 1.5 % in terms of ZMLD for all instruments. In addition, all the deviations are below 1σ , and can therefore be fully explained by random statistical dispersion. As a remark, the agreement between the VLTI/VINCI results and the Mk III is remarkable, with no systematic deviation detectable at a level of a few tenths of a percent. This is especially encouraging as these two instruments are observing at very different wavelengths (visible and K band, respectively).

This comparison exercise relies implicitly on the assumption that the considered $ZMLD_0(C_0 - C_1)$ relations are applicable to each instrument's subsample of stars, down to the precision of each individual measurement. This may not be the case for all stars, but the agreement that we observe is a worst case, and the true agreement is in any case very satisfactory.

7. Previous calibrations and other luminosity classes

Previous calibrations of the SB relations for dwarfs have been derived by Di Benedetto (1998) and Van Belle (1999a). These two authors relied on the limited sample of hot dwarfs observed with the Narrabri intensity interferometer (Hanbury Brown et al. 1974a; 1974b). The agreement of our calibration with the work by Van Belle (1999a) is satisfactory within 1σ for the $(V, V - K)$ relation, but there is a difference of about 2σ in the slope of the $(B, B - K)$ relation. As the fit obtained by this author is based on a small range of colors, we attribute this moderate discrepancy to an underestimation of the true error bar in the slope, even in the restricted quoted range of validity ($-0.6 \leq B - K \leq +2.0$).

Several calibrations of the SB relations for giants have been proposed in recent years, thanks to the availability of a number of direct interferometric measurements of this class of stars. Van Belle (1999a) used a sample of 190 giants, complemented by 67 carbon stars and Miras

Table 7. Comparison between interferometers. The average residuals of the fits of $ZMLD_B$ and $ZMLD_V$ for the K and L based colors are given together with the corresponding 1σ error bars. All values are expressed in percents of the $ZMLD$ values. All the residuals are compatible with zero within their 1σ error bars.

Instrument	N	$\Delta ZMLD_B(B - K)$	$\Delta ZMLD_V(V - K)$	$\Delta ZMLD_B(B - L)$	$\Delta ZMLD_V(V - L)$
PTI	5	$+0.48 \pm 0.89\%$	$+0.82 \pm 0.94\%$	$+0.63 \pm 0.89\%$	$+0.89 \pm 0.93\%$
NII	5	$+1.02 \pm 1.42\%$	$+1.03 \pm 1.46\%$	$+1.03 \pm 1.58\%$	$+1.02 \pm 1.63\%$
Mk III	11	$-0.11 \pm 0.56\%$	$-0.12 \pm 0.57\%$	$-0.06 \pm 0.64\%$	$-0.11 \pm 0.66\%$
NPOI	5	$-1.20 \pm 1.20\%$	$-1.23 \pm 1.24\%$	$-1.23 \pm 1.24\%$	$-1.39 \pm 1.53\%$
VLTI/VINCI	16	$-0.05 \pm 0.49\%$	$-0.07 \pm 0.51\%$	$-0.07 \pm 0.51\%$	$-0.11 \pm 0.68\%$

measured with the PTI (Van Belle et al. 1999b), IOTA (e.g. Dyck et al. 1998) and lunar occultation observations (e.g. Ridgway et al. 1982) to calibrate the $F_V(V - K)$ relation of giant and supergiant stars. Welch (1994) and Fouqué & Gieren (1997) proposed a calibration of the SB relations of Cepheids based on an extrapolation of the corresponding relations of giants. Among the supergiants, Cepheids occupy a particular place. The observations of these variable stars by interferometry, intended primarily to study their pulsation, have resulted in the measurement of several of these objects (Mourard et al. 1997; Lane et al. 2000; Nordgren et al. 2000; Kervella et al. 2001; Lane et al. 2002; Kervella et al. 2004b). Based on these observations, Nordgren et al. (2002) have established dedicated SB relations for Cepheids, and they find a satisfactory agreement with previous works. From these studies, it appears that the SB relations found for giants and supergiants are similar to the ones determined in the present paper for dwarfs and subgiants, especially their visible-infrared versions. This means qualitatively that any two stars of class I-V with similar magnitudes in two bands will present approximately the same angular diameters.

8. Main Sequence stars as calibrators for long-baseline interferometry

8.1. The need for small and nearby calibrators

Interferometric observations are generally based on interleaved observations of a scientific target and a calibrator. The angular size of the calibrator is supposed to be known *a priori*, and the observed fringe contrast is used to estimate the instrumental transfer function (also called system visibility). The catalogue of calibrators assembled by Cohen et al. (1999), and customized to interferometry by Bordé et al. (2002), consists mainly of K giants with angular diameters of about 2 mas. While this size is well adapted to short baseline observations (up to a few tens of meters in the infrared), these stars are too large angularly to serve as calibrators for the hectometric baselines of the VLTI, the CHARA array (McAlister et al. 2000) or the NPOI (Armstrong et al. 1998). In addition, it is foreseen that shorter wavelengths will be implemented on the VLTI than the K band currently accessible with VINCI. For instance, the AMBER instrument (Petrov et al. 2000) will allow observations in the J band. The two-fold increase in angular resolution will naturally require significantly

smaller calibrators than those in the Cohen et al. (1999) catalogue.

A fundamental problem with distant stars is that the reddening corrections are uncertain. This means that it is highly desirable to use nearby stars as calibrators, located within a few tens of parsecs. In this respect, giant stars are not well suited due to their large linear dimensions, but dwarfs and subgiants are ideally suited to provide small and well-defined calibrators.

Another advantage of Main Sequence stars is that their strong surface gravity results in a compact atmosphere and a well-defined photosphere. Their disk appears sharper than that of the giants, for which the precise definition of the limb darkened disk angular diameter at a level of less than 1% can be difficult, in particular for the later spectral types. As an example, a discussion of the M4III giant ψ Phe can be found in Wittkowski, Aufdenberg & Kervella (2004).

8.2. Calibration precision vs. brightness

It is possible to estimate the maximum angular size of calibrator stars in order to obtain a given relative precision in the calibration of the interferometric efficiency. Fig. 6 shows the achievable precision in the interferometric efficiency using the $(B, B - L)$ relation determined in Sect. 4.2 ($\sigma \leq 1.0\%$), as a function of the angular diameter of the calibrator star, for four different baselines (100, 200, 400 and 800 m), in the H band. These baselines are representative of the existing or foreseen interferometers (Keck, PTI, VLTI, CHARA, NPOI and OHANA, sorted by increasing maximum baseline). The horizontal scale of Fig. 6 can be adapted for other wavelengths or other baselines by scaling it linearly while maintaining constant the B/λ ratio.

If we now set a limit of 0.5% on the acceptable systematic uncertainty in the interferometric efficiency, we can compute the apparent magnitude of the Main Sequence calibrators that should be used as a function of their color. The result is presented in Fig. 7 as a function of the $B - H$ color, for different baseline lengths and interferometric observations in the H band. From this figure, it can be concluded that suitable calibrators for extremely long baseline observations will have to be faint. Let us consider the example of the OHANA interferometer (original idea proposed by Mariotti et al. 1996), whose longest foreseen

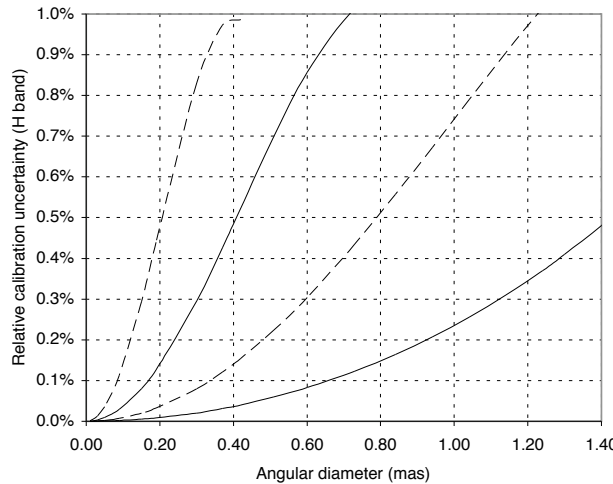


Fig. 6. Precision achievable in the measurement of the interferometric efficiency as a function of the angular diameter of the calibrator, predicted using the $(B, B - L)$ SB relation ($\leq 1.0\%$ dispersion). From left to right, the curves refer to baselines of 800, 400, 200 and 100 m, in the H band.

baseline is 800 m. The H band magnitude of the calibrators necessary to obtain a relative systematic visibility error of 0.5% will be between $m_H = 6$ and 8, depending on the spectral type. This is rather faint, even for large aperture light collectors, but it is feasible with OHANA.

As an alternative, it is possible to build (through time consuming observations) a secondary network of brighter and larger calibrators based on the small angular diameter ones, but there will always be a limitation attached to the fact that calibrators have to be observed in the first lobe of their visibility function. For OHANA, this sets a hard limit of $\simeq 0.5$ mas on the calibrator angular size, and even ≤ 0.4 mas to obtain a visibility of at least 0.3. This corresponds to apparent magnitudes of $m_H = 5$ to 7 in the H band, one magnitude brighter than the primary network.

For the longest baseline of the VLTI (200 m), calibrator magnitudes between $m_H = 3$ and 5 will be sufficient, clearly in the accessible domain of the AMBER beam combiner (Petrov et al. 2000) with the 1.8 m Auxiliary Telescopes (Koehler et al. 2002). The creation of a secondary network of calibrators should therefore not be necessary.

It should be stressed that the present conclusions regarding magnitudes are not limited to dwarf stars, as giants and supergiants follow comparable surface brightness relations. This means that the magnitude ranges defined above will be almost the same for other luminosity classes. A decisive advantage of dwarfs is that for the same apparent magnitude, they will be much closer than the more luminous classes, and therefore significantly less affected by interstellar extinction.

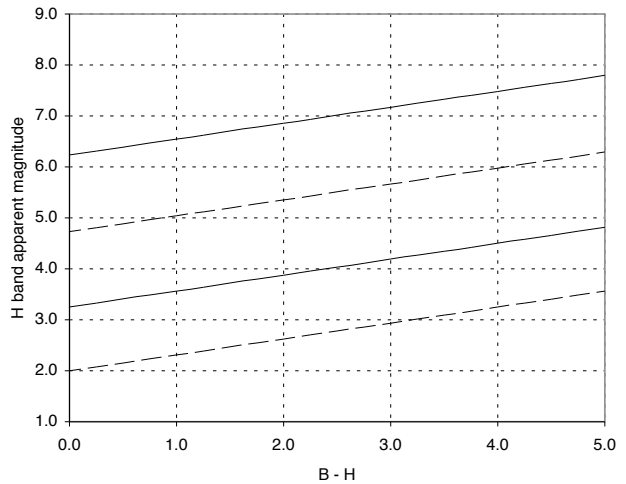


Fig. 7. Apparent magnitude in the H band of the calibrators suitable for obtaining a relative precision of 0.5% in the calibration of the interferometric efficiency, as a function of the $B - H$ color. From top to bottom, the curves refer to baselines of 800, 400, 200 and 100 m, in the H band.

Table 8. Photometry (upper part) and predicted limb darkened angular diameters θ_{LD} (lower part) of the planet-hosting stars 51 Peg A and HD 209458 A.

	51 Peg A	HD 209458 A
m_V	5.50 ± 0.01	7.65 ± 0.01
m_K	3.97 ± 0.01	6.31 ± 0.03
$\theta_{LD}(K, V - K)$	0.689 ± 0.011 mas	0.228 ± 0.004 mas

8.3. Example of diameter prediction

As a practical application, we have chosen the two stars 51 Peg A (HD 217014) and HD 209458 A. The former hosts the first planet discovered around a solar type star (Mayor & Queloz 1995), and the latter presents planetary transits (Charbonneau et al. 2000). We selected these two stars because they have been observed extensively using different techniques and did not show any large amplitude photometric variability. They therefore represent good examples of stable, well known stars, and are ideal candidates for the prediction of their angular size using the SB relations determined in the present paper.

Table 8 presents the predicted angular diameters of the two stars for the $(V, V - K)$ version of the SB relation. The m_V magnitudes are from *Hipparcos* (Perryman et al. 1997) for both stars, with an arbitrary error bar of ± 0.01 , while the K band infrared magnitudes were taken from Ducati et al. (2002) for 51 Peg A, and from the 2MASS catalogue (Cutri et al. 2003) for HD 209458 A.

For 51 Peg A, we obtain a predicted angular diameter of $\theta_{LD} = 0.689 \pm 0.011$ mas. The corresponding value for HD 209458 A is $\theta_{LD} = 0.228 \pm 0.004$ mas. These angular sizes can be translated into linear radii using the *Hipparcos* parallaxes (Perryman et al. 1997), $\pi_{51\text{ Peg A}} =$

65.10 ± 0.76 mas and $\pi_{\text{HD 209458 A}} = 21.24 \pm 1.00$ mas. We obtain $R_{51 \text{ Peg A}} = 1.138 \pm 0.023 R_{\odot}$ and $R_{\text{HD 209458 A}} = 1.154 \pm 0.059 R_{\odot}$. HD 209458 A is a particularly interesting object, as Brown et al. (2001) have been able to estimate directly its linear radius through the deconvolution of the light curve of the transit. They obtain a value of $R_{\text{HD 209458 A}} = 1.146 \pm 0.050 R_{\odot}$, in remarkable agreement with our (K , $V - K$) prediction. The bulk of the $\pm 5\%$ uncertainty comes from the error in the *Hipparcos* parallax, the relative error in the angular size being only $\pm 2\%$.

The direct measurement of the angular diameter of 51 Peg A is within the capabilities of the existing very long baseline interferometers (several hundred meters), but this is not true for HD 209458 A. Its 0.228 mas size would require baselines of more than 800 m to be resolved at visible wavelengths (several kilometers in the infrared). Such baselines are not presently available or scheduled. And even so, the calibration of these observations would be extremely difficult, as the calibrator would have to be very faint. More generally, carefully calibrated surface brightness relations are currently the only method to estimate precisely ($\pm 1\%$) the angular size of solar type stars fainter than $m_V = 7$.

9. Conclusion

The laws that we established between the angular size and broadband colors (or effective temperature) are strictly empirical. Our best relations present a very small intrinsic dispersion, down to less than 1%. They can be used to predict the angular sizes of A0–M2 dwarfs and A0–K0 subgiants from simple, readily available broadband photometry. On the one hand, Gray et al. (2003) have recently published an extensive survey of the spectral properties of nearby stars within 40 pc, including estimates of their effective temperatures. On the other hand, several large catalogues (2MASS, DENIS,...) provide high precision magnitudes of these stars in the infrared. From the cross-comparison of these sources, the SB relations determined in the present paper make it possible to assemble a catalogue of calibrators for interferometry that will be practically unaffected by interstellar extinction, multiplicity or circumstellar material biases. These resulting angular diameter predictions will provide a reliable basis for the calibration of long-baseline interferometric observations.

Acknowledgements. P.K. acknowledges partial support from the European Southern Observatory through a post-doctoral fellowship. D.S. acknowledges the support of the Swiss FNRS. This research has made extensive use of the SIMBAD and VIZIER online databases at CDS, Strasbourg (France).

References

Allende Prieto, C., Asplund, M., Garcia Lòpez, R. J., & Lambert, D. L. 2002, ApJ, 567, 544

Armstrong, J. T., Mozurkewich, D., Rickard, L. J., et al. 1998, ApJ, 496, 550

Barnes, T. G., Evans, D. S., & Parson, S. B. 1976, MNRAS, 174, 503

Bessell, M. S., Castelli, F., & Plez, B. 1998, A&A, 333, 231

Boden, A. F., Van Belle, G. T., Colavita, M. M. 1998, ApJ, 504, 39

Bordé, P., Coudé du Foresto, V., Chagnon, G., & Perrin, G. 2002, A&A, 393, 183

Brown, T. M., Charbonneau, D., Gilliland, R. L., Noyes, R. W., Burrows, A. 2001, ApJ, 552, 699

Cayrel de Strobel, G., Soubiran, C., Friel, E.D., Ralite, N., & Francois, P., 1997, A&AS, 124, 299

Cayrel de Strobel G., Soubiran C., & Ralite N. 2001, A&A, 373, 159

Cenarro, A. J., Cardiel, N., Gorgas, J., et al. 2001, MNRAS, 326, 959

Charbonneau, D., Brown, T. M., Latham, D. W., & Mayor, M. 2000, ApJ, 522, L145

Ciardi, D. R., Van Belle, G. T., Akeson, R. L., et al. 2001, ApJ, 559, 1147

Claret, A. 2000, A&A, 363, 1081

Cohen, M., Walker, R. G., Carter, B., et al. 1999, AJ, 117, 1864

Colavita, M. M., Wallace, J. K., Hines, B. E., et al. 1999, ApJ, 510, 505

Colina, L., Bohlin, R. C., & Castelli, F. 1996, AJ, 112, 307

Cutri, R. M., Skrutskie, M. F., Van Dyk, S., et al. 2003, Univ. of Massachusetts and IPAC, <http://www.ipac.caltech.edu/2mass>.

Davis, J., & Tango, W. J. 1986, Nature, 323, 234

Di Benedetto, G. P. 1998, A&A, 339, 858

Di Folco, E., Thévenin, F., Kervella, P., et al. 2004, *in prep.*

Domiciano de Souza, A., Kervella, P., Jankov, S., et al. 2003, A&A, 407, L47

Ducati, J. R. 2002, NASA Ref. Pub. 1294

Dyck, H. M., Van Belle, G. T., & Thompson, R. R. 1998, AJ, 116, 981

Erspamer, D., & North, P. 2003, A&A 398, 1121

Fouqué, P., & Gieren, W. P. 1997, A&A, 320, 799

Fouqué P., Chevallier, L., Cohen, M., et al. 2000, A&AS, 141, 313

Glass, I. S. 1974, Month. Not. of Astron. Soc. South Africa, 33, 53

Glass, I. S. 1975, MNRAS 171, 19

Glindemann, A., Abuter, R., Carbognani, F., et al. 2000, Proc. SPIE, 4006, 2

Glindemann, A., Argomedo, J., Amestica, R., et al. 2003a, Proc. SPIE, 4838, 89

Glindemann, A., Argomedo, J., Amestica, R., et al. 2003b, ApSS, 286, 1

Gray, R. O., Graham, P. W., & Hoyt, S. R. 2001, AJ, 121, 2159

Gray, R. O., Corbally, C. J., Garrison, R. F., Mc Fadden, M. T. & Robinson, P. E. 2003, AJ, 126, 2048

Hanbury Brown, R., Davis, J., Allen, L. R. 1967, MNRAS, 137, 375

Hanbury Brown, R., Davis, J., Lake, J. W., & Thompson, R. J. 1974a, MNRAS, 167, 475

Hanbury Brown, R., Davis, J., & Allen, L. R. 1974b, MNRAS, 167, 121

Hoffleit, D., & Warren W. H. 1991, The Bright Star Catalogue, 5th Revised Ed., Astronomical Data Center, NSSDC/ADC

Kervella, P., Coudé du Foresto, V., Glindemann, A., Hofmann, R. 2000, Proc. SPIE, 4006, 31

Kervella, P., Coudé du Foresto, V., Perrin, G., et al. 2001, A&A, 367, 876

Kervella, P., Gitton, Ph., Ségransan, D., et al. 2003a, Proc. SPIE, 4838, 858

Kervella, P., Thévenin F., Morel P., Bordé, P., & Di Folco, E. 2003b, A&A, 408, 681

Kervella, P., Thévenin, F., Ségransan, D., et al. 2003c, A&A, 404, 1087

Kervella, P., Thévenin F., Morel P., et al. 2004a, A&A, 413, 251

Kervella, P., Nardetto, N., Bersier, D., Mourard, D., & Coudé du Foresto V. 2004b, A&A, 416, 941

Kidger, M. R., & Martín-Luis, F. 2003, AJ, 125, 3311

Koehler, B., Flebus, C., Dierickx, P., et al. 2002, ESO Messenger, 110, 21

Kurucz, R. L. 1992, IAU Symp. 149: The Stellar Populations of Galaxies, 149, 225

Lane, B. F., Kuchner, M. J., Boden, A. F., Creech-Eakman, M., & Kulkarni S. R. 2000, Nature, 407, 485

Lane, B. F., Boden, A. F., & Kulkarni, S. R., 2001, ApJ, 551, L81

Lane, B. F., Creech-Eakman, M., & Nordgren, T. E. 2002, ApJ, 573, 330

Leggett, S. K. 1992, ApJS, 82, 35

Mariotti, J.-M., Coudé du Foresto, V., Perrin, G., Peiqian Zhao, & Léna, P., 1996, A&AS, 116, 381

McAlister, H. A., Bagnuolo, W. G., ten Brummelaar, T. A., et al. 2000, Proc. SPIE, 4006, 465

Mayor, M., & Queloz, D. 1995, Nature, 378, 355

Mermilliod J.-C. 1986, Catalogue of Eggen's UVB data (unpublished, available through SIMBAD)

Morel, M., & Magnenat, P. 1978, A&AS, 34, 477

Morel, P., Provost, J., Lebreton, Y., Thévenin, F., & Berthomieu, G. 2000, A&A, 363, 675

Morel, P., Berthomieu, G., Provost, J., & Thévenin, F. 2001, A&A, 379, 245

Mould, J. R., & Hyland A. R. 1976, ApJ, 208, 399

Mourard, D., Bonneau, D., Koechlin, L., et al. 1997, A&A, 317, 789

Mozurkewich, D., Armstrong, J. T., Hindsley, R. B., et al. 2003, AJ, 126, 2502

Nordgren, T. E., Germain, M. E., Benson, J. A., et al. 1999, AJ, 118, 3032

Nordgren, T. E., Armstrong, J. T., Germain, M. E., et al. 2000, ApJ, 543, 972

Nordgren, T. E., Sudol, J. J., & Mozurkewich, D. 2001, AJ, 122, 2707

Nordgren, T. E., Lane, B. F., Hindsley, R. B., & Kervella, P. 2002, AJ, 123, 3380

Ochsenbein, F., Bauer, P., Marcout, J. 2000, A&AS, 143, 221

Pasinetti-Fracassini, L. E., Pastori, L., Covino, S., & Pozzi, A. 2001, A&A, 367, 521

Petrov, R., Malbet, F., Richichi, A., et al. 2000, Proc. SPIE, 4006, 68

Perryman, M. A. C., Lindegren, L., Kovalevsky, J., et al., *The Hipparcos Catalogue*, 1997, A&A, 323, 49

Ridgway, S. T., Jacoby, G. H., Joyce, R. R., & Wells, D. C., 1982, AJ, 87, 1044

Shao, M., Colavita, M. M., Hines, B. E., et al. 1988, ApJ, 327, 905

Ségransan, D., Kervella, P., Forveille, T., Queloz, D. 2003, A&A, 397, L5

Ségransan, D., Kervella, P., et al., in preparation

Söderhjelm, S. 1999, A&A 341, 121

Thévenin F., & Idiart, T. P. 1999, ApJ, 521, 753

Thévenin, F., Kervella, P., et al., in preparation

Van Belle, G. T. 1999a, PASP, 111, 1515

Van Belle, G. T., Lane, B. F., Thompson, R. R., et al. 1999b, AJ, 117, 521

Welch, D. L. 1994, AJ, 108, 1421

Wittkowski, M., Aufdenberg, J. P., & Kervella, P. 2004, A&A, 413, 711